Improving electron and ion transport by constructing 3D graphene nanosheets sandwiched between porous carbon nanolayers produced from resorcinol-formaldehyde resin for high-performance supercapacitor electrodes

SUN Bing[1,2,†], TANG Wen[1,2,†], XIANG Hui[2], XU Wen-li[1,2], CONG Ye[1,2], YUAN Guan-ming[1,2], ZHU Hui[1,2], ZHANG Qin[1,2,*], LI Xuan-ke[1,2,*]

(1. *The State Key Laboratory of Refractories and Metallurgy*, *Wuhan University of Science and Technology*, *Wuhan*, 430081, *China*;
2. *School of Chemistry and Chemical Engineering*, *Wuhan University of Science and Technology*, *Wuhan* 430081, *China*)

Abstract: An ideal supercapacitor electrode should contain three-dimensional (3D) interpenetrating electron and ion pathways with a short transport distance. Graphene-based carbon materials offer new and fascinating opportunities for high performance supercapacitor electrodes due to their excellent planar conductivity and large surface area. 3D graphene nanosheets coated with carbon nanolayers of controllable thickness from resorcinol-formaldehyde (RF) resin are constructed and activated by KOH to develop pores. Such a sandwich structure provides abundant transport channels for ions with short paths. The porous carbon nanolayers accelerate ion transport, while the graphene networks improve the conductivity, boosting electron transport. As expected, the prepared porous carbon has a high surface area of 690 $m^2\ g^{-1}$ and a high specific capacitance of up to 324 $F\ g^{-1}$ in a 6 mol L^{-1} KOH aqueous electrolyte at a current density of 0.2 $A\ g^{-1}$. More than 99% of the capacitance is retained after 8 000 charge–discharge cycles at a high current density of 5 $A\ g^{-1}$, indicating good cycling stability. This research provides an effective strategy for the development of outstanding electrode materials for the enhanced transport of both electrons and ions.

Key words: Graphene-based nanosheet; Hierarchical porous structure; Controllable thickness; Supercapacitor

1 Introduction

Supercapacitors (SCs), a kind of the most prospective energy storage devices, have received considerable critical attentions owing to their merits of high power density, long cyclic life and rapid charge-discharge when they are served in power source and digital device applications[1–3]. Previous Studies have witnessed wide utilization of graphene equipped with high specific surface area (2 630 $m^2\ g^{-1}$) and superior conductivity in SCs electrodes[4]. Since the stacking and aggregation of graphene layers were induced by strong van der Waals interlayer interaction[5], graphene was partly restricted on specific surface area and electrochemical performance, failing to exert its theoretical outstanding capacitance.

Coating conductive polymers (CPs) on the surface of graphene oxide (GO), such as polyaniline[6,7], polypyrrole, and 3,4-ethylenedioxythiophene[8,9], were considered as an effective strategy to alleviate the aggregation and stacking of GO sheets. Moreover, a dramatic increase in specific capacitance of CPs-GO composite occurred, resulting from the contribution of pseudo-capacitive and electric double layer capacitive (EDLC) behavior[10]. However, slight aggregation of GO still exists during the postprocessing procedure. It becomes worse when CPs have low water solubility, especially. CPs cannot be well coated on the surface of GO. Furthermore, the huge volume expansion of CPs leads to a decay in their electrochemical performance during the charge-discharge process[11–13]. Considering this issue, microporous polymer networks, such as phenol-formaldehyde resin and resorcinol-

Received date: 2020-09-10; **Revised date:** 2020-10-14

Corresponding author: ZHANG Qin, Ph. D, Associate Professor. E-mail: zhangqin627@wust.edu.cn;
LI Xuanke, Ph. D, Professor. E-mail: xkli8524@sina.com

Author introduction: SUN Bing, Ph. D candidate. E-mail: bsun1010@sina.cn;
TANG Wen, Master student. E-mail: wttangwen@163.com. †These authors contributed equally to this work.

Supplementary data associated with this article can be found in the online version.

formaldehyde resin[14,15], were adopted to coat on the surface of GO to form a sandwich structure. For instance, Zhu and his co-workers reported a porous sandwich-like carbon/graphene nanosheets, possessing an ultrahigh surface area of 2 650 $m^2\ g^{-1}$[16]. Nonetheless, such a high surface area failed to exhibit an ideal capacitance (only 116 F g^{-1} at 0.5 A g^{-1} in 6 mol L^{-1} KOH), owing to its unsuitable pore size distribution. Hao et al. also reported the microporous carbon nanosheets sandwiched by GO, which delivered a poor capacitance of 105 F g^{-1} at 0.5 A g^{-1}[17]. In the study, it has no knowledge of the relationship between thickness of carbon and ions, electrons transport. Obviously, controlling the thickness of carbon coating is a crucial factor for promoting electronic transportation and pore utilization of graphene-based sheets. Thus, it is no denying that constructing a graphene-based nanosheet with microporous carbon coating, as well as controlled thickness and pore size distribution, is of great significance to rapid ion and electron transportation.

Herein, a hierarchically porous carbon/graphene/carbon nanosheet, inspired by a cheese sandwich, was facilely prepared. RF-resin was well coated on both sides of GO via a controllable preparation process. GO and RF-resin were connected by electrostatic interaction and hydrogen-bond interaction, resulting in an effective restriction in stacking and aggregation of the graphene sheets. The abundant porous structure of the precursors was formed after pyrolysis and followed by KOH activation. High specific surface (690 $m^2\ g^{-1}$) and thin thickness (15 nm) 2D graphene-based nanosheets with narrow pore size distribution were prepared, which are favorable to the accessibility of the electrolyte and fast electrons transfer. Benefited from the effective synthesis strategy, the obtained composites exhibited high capacitance and excellent cycle stability.

2 Experimental

2.1 Synthesis of the porous C/G nanosheets

GO was prepared by a modified Hummer's method[18], and then, it was dispersed into deionized (DI) water to get a homogeneous GO aqueous solution of 2.50 mg mL^{-1}. The materials preparation process was described as follows. 2.72 mL of GO aqueous solution was dispersed into 2.28 mL of deionized water and 4 mL of anhydrous ethanol by ultrasonic, then the solution was mixed with 0.46 mL of resorcinol (AR, 99%, Aladdin Industrial corporation) aqueous solution of 250 mg mL^{-1}. 60 μL of $NH_3 \cdot H_2O$ (Sinopharm Chemical Reagent Co., Ltd), 0.38 mL of Pluronic F127 (Mw = 12 600, $PEO_{106}PPO_{70}PEO_{106}$, Aldrich Corp, 100 mg mL^{-1}) and 0.16 mL of formaldehyde (37 wt.%, Sinopharm Chemical Reagent Co., Ltd) were mixed with the magnetic stirring at 25 °C for 1 h. The homogeneous emulsion was then sealed and transferred into an oven at 90 °C for 8 h. The precursor was dried in the vacuum freeze-drying and annealing at 650 °C for 2 h under N_2 atmosphere. And then, the hierarchically porous sandwich-like carbon/graphene/carbon nanosheets (donated CGS) were obtained.

The surface area is a key point for the high-performance of supercapacitor. Therefore, KOH chemical activation is the second step to enrich the pores of CGS. Typically, KOH (AR, Sinopharm Chemical Reagent Co., Ltd) was dissolved in 20 mL of deionized (DI) water and the dried CGSs were dispersed into the solution with sonication for 30 min. The mass ratio of KOH/CGS is 1∶1. The impregnated sample was dried at 100 °C in an oven and then activated at objective temperature (400, 600, 800 °C) for 2 h respectively. After it was cooled down, an excessive 0.5 mol L^{-1} HCl was used to remove the KOH. Subsequently, samples were repeatedly washed with DI water to remove remaining inorganic salt with the pH7 of the filtrates. The product (denoted KACGS-T, where T represents the activation temperature) was dried in an oven at 100 °C for 24 h.

2.2 Materials characterization

The micrographs were observed by scanning electron microscopy (SEM) using a Helios NanoLab 600i instrument. Transmission electron microscopy (TEM) images were obtained with a Tecnai G2 F20 electron microscope. X-ray diffraction (XRD) pat-

terns were recorded with an Advance D8 using Cu *Kα* radiation. The Raman analyses of the samples were performed on a Lab RAM HR800 laser Raman spectrometer. The specific surface area and porous distribution were measured with an ASAP 2020 sorption analyzer.

2.3 Electrochemical measurements

The electrochemical performances were measured by using a three-electrode system at 25 °C. To make the working electrodes, 90 wt.% of active materials and 10 wt.% of poly-tetrafluoroethylene (PTFE) binder were dispersed in a mixed solution of DI water and ethanol (1/5, by volume) with the sonication for 30 min. The slurry was dried in the oven at 80 °C for 4 h and the mixture was laminated to a flake. Afterward, the as-electrodes (d = 1.2 cm) were dried in the vacuum oven at 80 °C for overnight and pressed it on a piece of nickel foam (1.2 cm×1.2 cm) under 5 MPa for 3 min. Each electrode contains about 5 mg of active materials. The electrodes were immersed in 6 mol L^{-1} KOH solution under 60 Pa for 10 h to make sure the electrodes sufficient contact with electrolyte.

Cyclic voltammetry (CV), Galvanostatic charge-discharge (GCD), and electrochemical impedance spectroscopy (EIS) was measured by a Gamry interface 1000E electrochemical workstation. All the electrochemical performances were studied in a three-electrode system using the above electrode as a working electrode, a platinum film as a counter electrode, and a mercuric oxide electrode as a reference electrode. The CV test was carried out with a potential window of −1 ~ 0 V vs Hg/HgO and the scan rate range of 5-200 mV s^{-1}. EIS was measured in the frequency range of 0.01-10^5 Hz at 5 mV amplitude. The GCD test had the same potential window of CV and the current densities range from 0.2 to 5 A g^{-1}.

The specific capacitance was respectively calculated by the GCD and CV tests result using the following equation:

$$C = I\Delta t/m\Delta V \quad (1)$$

Where C (F g^{-1}) is the specific capacitance, I is the discharge current (A g^{-1}), t is the discharging time (s), m is the mass of active materials in one electrode (g) and V is the voltage drop upon discharging (excluding the IR drop).

$$C = \int i\mathrm{d}v/m\,v\,V \quad (2)$$

Where C (F g^{-1}) is the specific capacitance, I is the output current (A), V is the potential (V), v is the potential scanning rate (mV s^{-1}) and m is the mass of the active material in the electrodes (g).

3 Results and discussion

Fig. 1a shows the schematic illustration of the preparation process of sandwich-like hierarchical porous carbon/graphene/carbon nanosheets. GO was used as a substrate, $NH_3{\cdot}H_2O$ and tri-block co-polymer F127 were used as the effective binder for fixing RF-resin on both sides of the substrate. Then, RF-resin was directly polymerized on the both sides of GO. The self-assembly of the micelle and RF oligomers induced the formation of micropores, mesopores and macropores. Meanwhile, a series of multilevel phase was separated in the polymerization process of RF resin. Subsequently, CGS was obtained after vacuum freeze-drying and pyrolysis under N_2 atmosphere. CGS was further activated by KOH to enrich their pore structures. Finally, the thin sandwich-like graphene-based nanosheets with rich microporous, plentiful mesoporous and macropores were formed. These features may shorten the pathway of the ion diffusion and enhance electron conduction. The macroscopic feature of CGS was shown in Fig. 1b. Three-dimension carbon frameworks can be obtained and the mass density of CGS is about 14.86 mg cm^{-3}, which is lightweight on the top of a flower. Fig. S1a shows the GO with the aggregated structure due to the van der Waals forces between the GO sheets. Obviously, without GO, the carbon derived from RF-resin (RFC) shows a typically self-assembly state of the regular balls (Fig. S1b)[19], and it is also confirmed by TEM images in Fig. S2. As seen in Fig. 1c, the obtained CGS shows a lamellar feature which has a smooth surface with interconnected structure. It indicates that

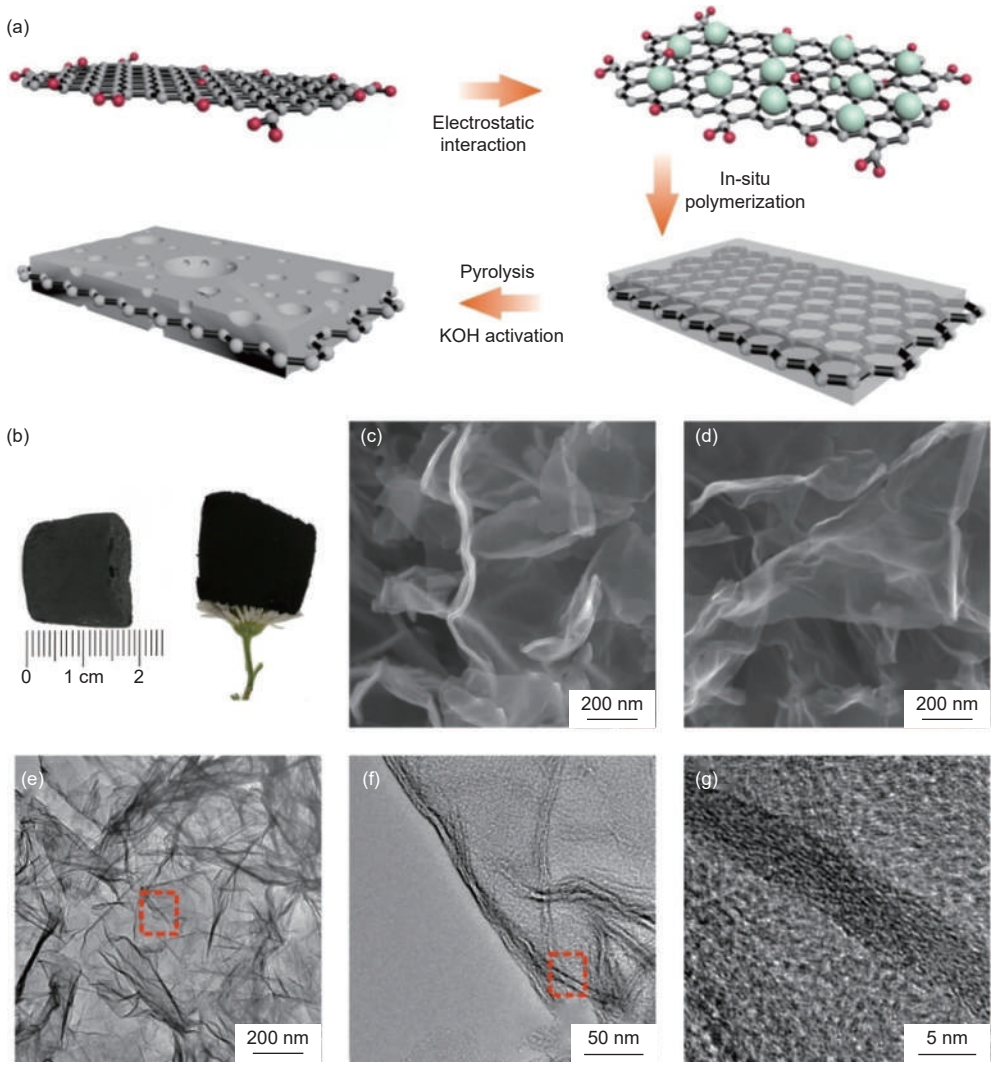

Fig. 1　(a) Schematic illustration of preparation process of sandwich–like and hierarchical porous carbon/graphene nanosheets, (b) macroscopic feature of CGS, (c) SEM image of original CGS, (d) SEM image of KACGS, (e–f) TEM images of KACGS, (g) HRTEM image of KACGS.

the RFC is homogeneously coated on the surface of graphene, which can effectively avoid the stacking of thin graphene nanosheets. And no ball-like resin carbon was observed in CGS.

For supercapacitor, the specific surface area plays an important role in the electrochemical performances[20,21]. Therefore, the prepared CGS is activated by KOH chemical activation to enrich their pore structures. KACGS still exhibited graphene-like interlinked structure shown in Fig. 1d, indicating the stable structure of KACGS. The TEM images of KACGS , shown in Fig. 1e and f, display the thin nanosheet morphologies, manifesting well dispersion of graphene after coating. Further, the hybrid features and detailed texture characteristics were observed by HRTEM. As shown in Fig. 1g, the interlayer with a distinct lattice fringe is GO, and both sides show the amorphous carbon texture with a large amount of micropores, illustrating a typical sandwich-like structure of KACGS.

The microstructure of the samples was further characterized by Raman spectroscopy and XRD analyses. Fig. 2a displays the Raman spectra of GO, CGS and KACGS. 2 peaks can be observed at 1 338 cm^{-1} and 1 588 cm^{-1}, corresponding to the defective/discorded sp^3 hybridized carbon (*D* band) and the in-plane stretching of sp^2 carbon bonds in the graphite planes (*G* band)[22], respectively. As is well known, the intensity ratio of the *D* band to the *G* band (I_D/I_G) is the reference of the disorder degree of carbon[23,24]. The

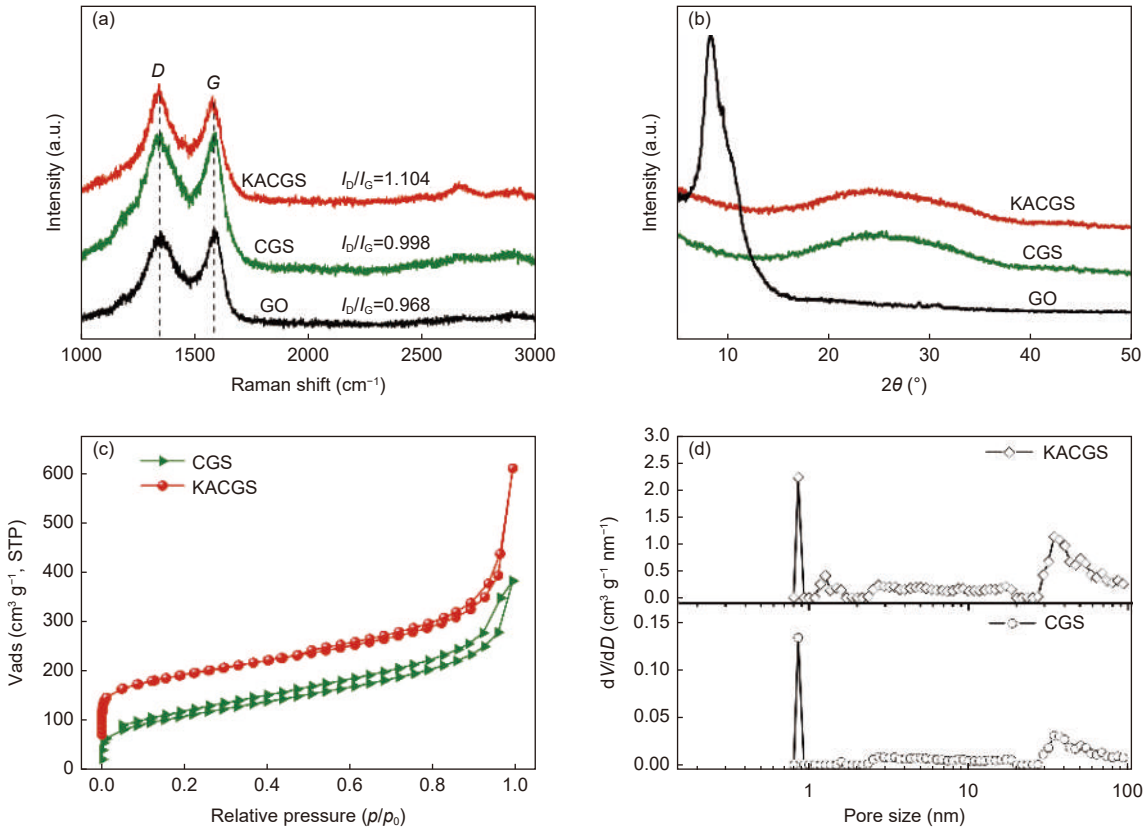

Fig. 2 (a) Raman spectra and (b) XRD patterns of GO, CGS and KACGS, (c) N_2 adsorption/desorption isotherms and (d) pore size distribution curves of CGS and KACGS.

I_D/I_G values of GO, CGS, and KACGS are 0.968, 0.998 and 1.104, respectively. The result is consistent with the typical amorphous porous carbons, demonstrating that more defects are formed after the KOH activation. Distinctly, the formation of more micropores in the RF-resin carbon texture gives rise to an increasing degree of defects. The structure of GO, CGS, and KACGS was further verified by XRD spectroscopy measurement (Fig. 2b). The XRD pattern of GO shows a diffraction peak at around 2θ of 8.2°, corresponding to the (001) diffraction peak of GO[25]. But the peak at 2θ of 8.2° disappears in CGS after the GO coated with RF-base carbon, and a new broad peak at 2θ of 24.9° is observed corresponding to d_{002} spacing of 0.357 nm. Based on the analysis, the amorphous structure of carbon coating in KACGS can be confirmed. According to N_2 adsorption/desorption measurements results (Fig. 2c and d), the hierarchically porous structure of prepared CGS and KACGS was confirmed by the isotherms shown type Ⅳ characteristics[26]. The adsorbed volumes of both increase rapidly and reache saturation soon at the low relative pressure $p/p_0 < 0.1$, reflecting the rich micropores of CGS and KACGS[27]. The obvious hysteretic loop at the high p/p_0 region suggests the mesopores existing in samples. The BET specific surface area of CGS was promoted from 330 to 690 m^2 g^{-1} (KACGS) after the activation with KOH. The pore size distribution is in the range of 0.8 to 125 nm. However, the main volume fraction is attributed to pores with diameters of 0.8 and 34.6 nm, confirming the hierarchical porous structure of the samples. In comparison with the pore volume of 0.59 cm^3 g^{-1} of CGS, the pore volume of KACGS increases to 0.94 cm^3 g^{-1}. The generation of such microporous features could be attributed to surface activation by KOH. A higher pore volume of KACGS manifests an increased exposure of active sites for ions adsorption in the micropores of electrode, and the mesopores contributes to the mass transportation, thus resulting in a high capacitance.

To explore the effect of RFC thickness on their electrochemical performance, CGSs with different

thicknesses of RFC were prepared. The obtained CGSs (Fig. 3,) possess thin RFC with an average thickness of 5.5, 26 and 37 nm on one side, corresponding to the CGS, 4d-CGS and 8d-CGS, respectively. The thickness of RFC was controlled by adjusting the mass ratio of GO and RF-resin. When the mass ratio of RF-resin increases to 8 times of the original ratio, little RFC balls can be observed in 8d-CGS (Fig. 3e). Furthermore, the obvious sandwich-like nanosheets can be seen, and RFC was tightly coated on both sides of GO, showing the successful prepare strategy. As the primary factors for capacitive behaviors, ionic and electronic transportation are closely connected with the diffusion length and resistance, respectively, which are influenced by the thickness of nanosheets.

As mentioned above, attributed to the hierarchically porous structure and the well pronounced 2D morphology, the prepared composites would be anticipated to perform electrolyte-accessibility and fast electron transport with the aid of the graphene framework. The CGS would be a promising candidate for supercapacitor electrode material. Therefore, the electrochemical properties of the prepared materials were investigated by cyclic voltammetry (CV), galvanostatic charge-discharge (GCD) and electrochemical impedance spectra (EIS) techniques using a three-electrode system. The electrolyte of 6 mol L^{-1} KOH aqueous solution was employed. Fig. S3 shows the GCD curves of CGSs with different thicknesses at a current density of 1 A g^{-1}. The specific capacitance of CGS, calculated from GCD curves, delivers a capacitance of 173.8 F g^{-1} at 1 A g^{-1}, which is much higher than that of 4d-CGS (72 F g^{-1}) and 8d-CGS (53 F g^{-1}). The internal resistance voltage drop (IR drop) reflected the contact resistance and rate of ion transport, which can be calculated by the abrupt potential drop in the discharge progress[28]. The IR drop for CGS, 4d-CGS and 8d-CGS was 0.018, 0.218 and 0.335V, respectively, showing that there is a positive correlation between the thickness of CGSs and the IR drop. CV curves of CGSs (Fig. S4) show that the integral areas decreased with increasing of the thickness of RFC, indicating a high capacitance in CGS. Nyquist plots of the three samples (Fig. S5) show that CGS and 4d-CGS have capacitive behaviors because of the vertical curves in the low-frequency region. According to the equivalent circuits, the CGS exhibits the lowest ohmic resistance and charge transfer resistance. Therefore, a rational decreasing in the thickness of carbon coating benefits for electron and ion transport, resulting in a high capacitance.

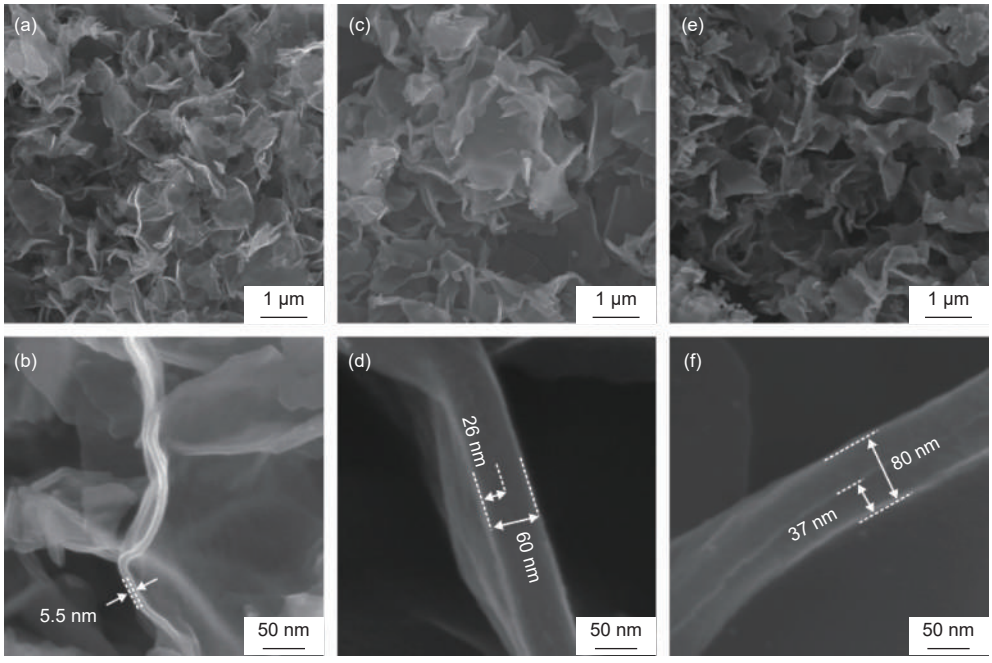

Fig. 3　SEM images of CGSs with different thicknesses of RFC, (a, b) CGS, (c, d) 4d–CGS and (e, f) 8d–CGS.

Furthermore, the specific capacitances of GO, RFC, CGS, and KACGS were compared base on the GCD measurement at the current density of 1 A g^{-1} (Fig. 4a). Their specific capacitances are calculated by Eq (1). The results show that the pure GO electrode exhibits much shorter discharging time and the lowest specific capacitance, indicating that the pores on GO nanosheets are useless caused by the aggregation of GO sheets. GO, RFC, CGS, and KACGS delivered specific capacitances of 23, 46, 172 and 223 F g^{-1} at 1 A g^{-1}, respectively. It can be proposed that the rich microporous carbon nanosheets with optimized thickness provide a short diffusion path for electrolyte penetration, and exert the conductivity of graphene for electron transport.

A wide range of prior studies proposed that high surface area and developed pore structure could ensure its superior capacitive behavior because the large surface area benefit for ion adsorption and the moderate pore structure promotes ion diffusion. Controlling the activation temperature is a crucial method to regulate surface area and pore structure. But excessive temperature causes the collapse of the microporous structure, resulting in a decrease in specific surface area. Therefore, the electrochemical performances of KACGS activated under varying temperatures were also investigated. As shown in Fig. S6, the shapes of the CV curves for KACGS and KACGS-800 exhibit a rectangular shape, indicating the EDLC behavior. The GCD curves (Fig. S7) for KACGSs were measured at a current density of 1 A g^{-1}. The linear nature of the GCD curves also demonstrates the EDLC feature of the electrode materials. And a more symmetric GCD curve of KACGS is observed, it exhibits a specific capacitance of 223.5 F g^{-1} ,which is much higher than that of KACGS-400 of 141 F g^{-1} and KACGS-800 of 199.3 F g^{-1}. As the current density increases from 0.2 to 5 A g^{-1}, the KACGS exhibits an excellent rate performance and retains 62.96% of its initial capacitance at 5 A g^{-1} (170 F g^{-1}), higher than that of KACGS-400 (8.33%) and KACGS-800 (58.22%).

The CV curves of GO, RFC, CGS and KACGS

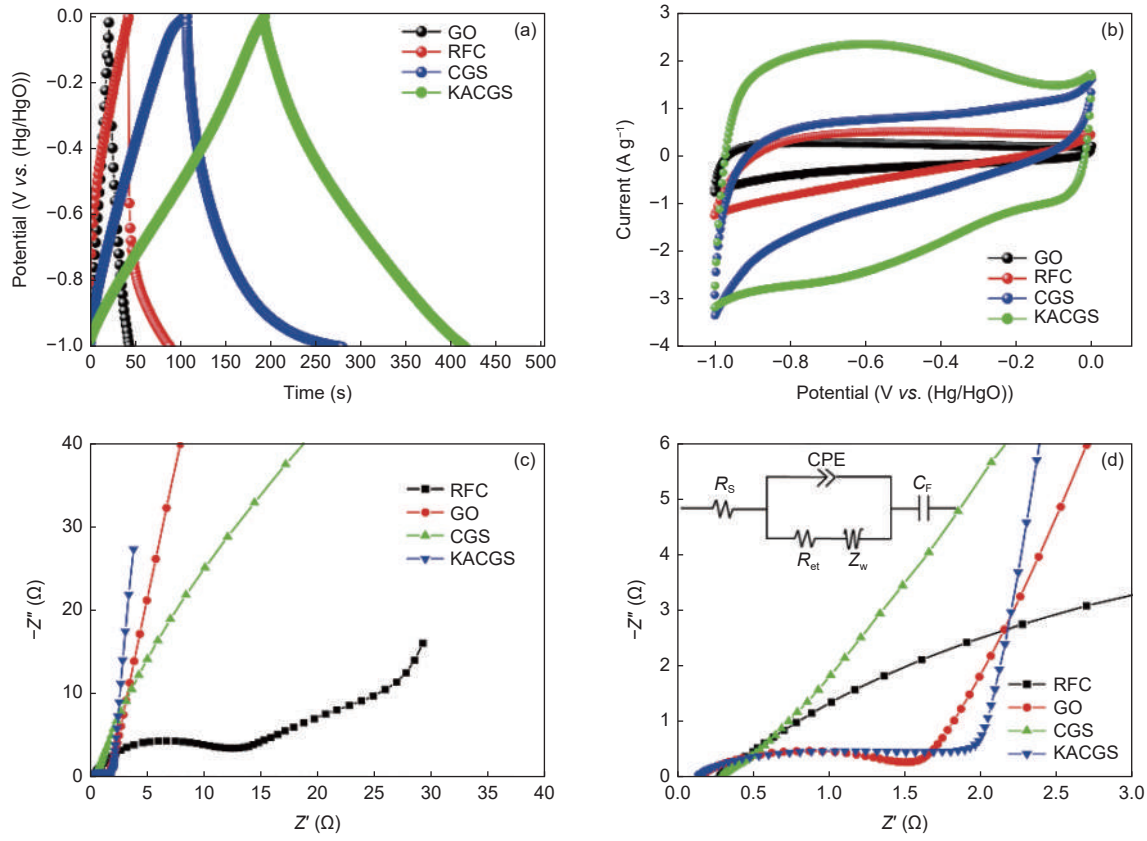

Fig. 4 (a) Galvanostatic charge/discharge cycling at constant currents of 1 A g^{-1}, (b) cyclic voltammograms at scan rate of 10 mV s^{-1}, (c, d) Nyquist plots of the experimental impedance data for GO, RFC, CGS and KACGS.

(Fig. 4b) show analogous rectangular curves from −1 to 0 V. Depending on Eq (2), the area of CV curves can be calculated which are similar to GCD results. Electrochemical impedance spectra of GO, RFC, CGS, and KACGS are further analyzed by Nyquist plots, which can reflect the contact resistance, charge transfer resistance, and the diffusion resistance of the ion in pores under the corresponding frequency region[17,28]. For the Nyquist plot (Fig. 4c), in the low-frequency region, the nearly vertical line reflects the capacitive behavior of an ideal capacitor. In the high-frequency region, the first intersection of semicircle and Z' axis reveals the internal resistance (R_s), The small semicircle shapes reflects the small charge transfer resistance (R_{ct}). An equivalent circuit model (inset of Fig. 4d) was shown to simulate the capacitive and resistive units in the supercapacitor system. It contains R_s, R_{ct}, the Warburg impendence (Z_w), which results from the diffusion resistance for the ion transfer in the electrode, the capacitance of contact interface (C_F), and the capacitance inside pores (CPE). All the samples have a small R_s (0.13-0.28 Ω). The RFC has a much larger R_{ct} value (11.6 Ω) and diffusion resistance than others. On the contrary, the GO and KACGS have a small diameter of the semicircle corresponding to the low R_{ct} of 1.56 and 1.72 Ω, respectively. The CGS electrode shows a smaller R_{ct} than GO and KACGS, due to the aggregation of GO and structural defect in KACGS by the activation of KOH. It indicates that the bulk conductive framework constructed from graphene and microporous carbons promotes the electrons transport, provides enough ionic transfer channel, and shortens ionic diffusion pathway during the electrochemical processes, and further gives rise to the outstanding energy storage performance.

To clearly understand the capacitive behavior of KACGS, the CV curves of different scan rates were shown in Fig. 5a. A rectangular shape curve can be observed at a low scan rate of 5 mV s^{-1}, indicating a good capacitive behavior. However, the shape of curves can't maintain with the increasing of scan rate

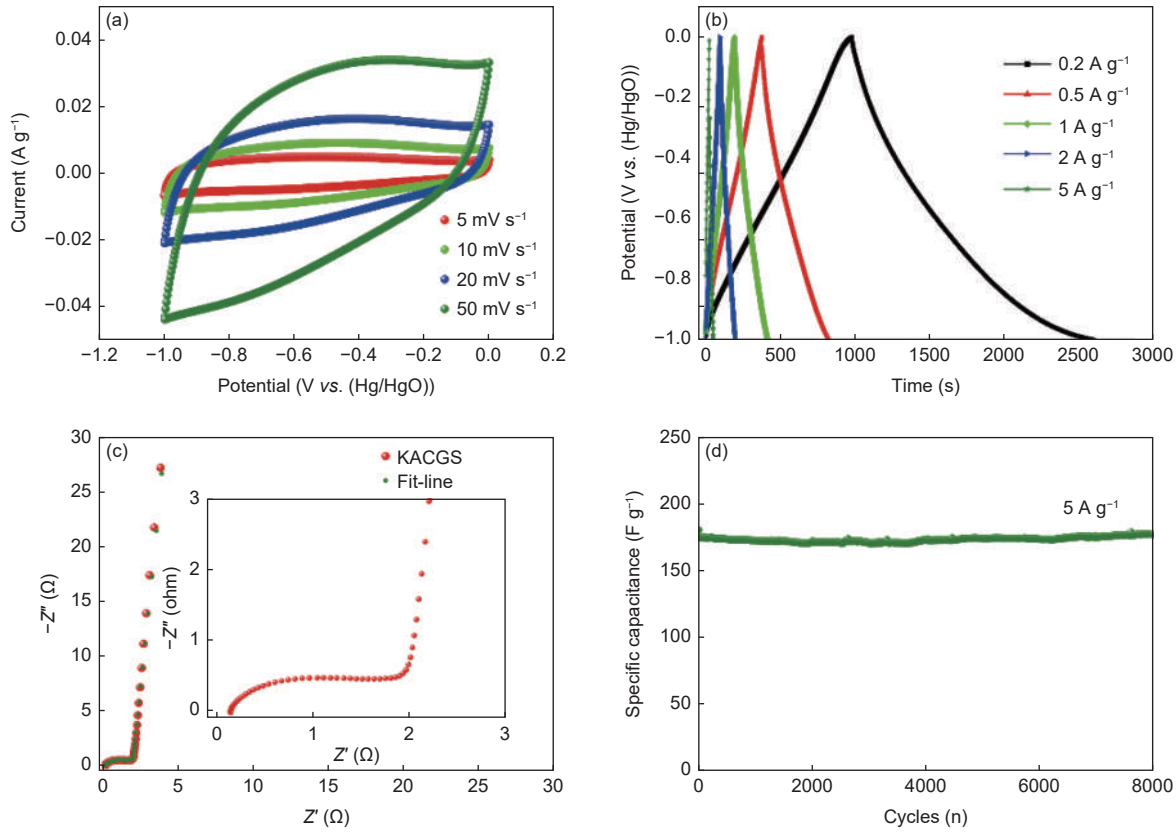

Fig. 5　Electrochemical performances of KACGS, (a) cyclic voltammograms at different scan rates, (b) galvanostatic charge/discharge cycling at different currents densities, (c) nyquist plots of the experimental impedance data, the inset shows the expanded high–frequency region of the plots (10 mHz to 100 kHz, ac amplitude, 5 mV). (d) cycling stability tests (8 000 cycles) at current density of 5 A g^{-1} within the potential window range from 0 to –1 V.

because the charging-discharging process is mainly governed by reversible K^+ ion adsorption and desorption on the surface of the porous carbon nanosheets in the aqueous KOH electrolyte[29]. The galvanostatic charge/discharge cycling curves of KACGS at various current densities are shown in Fig. 5b. The quasi triangular shape of the curves at 0.2 A g^{-1} reveals the EDLC behavior and the long discharging time suggests the high specific capacitance of 324 F g^{-1}, calculated from the discharged curves by Eq (1). However, the little curved discharging curves indicate the contribution of pseudo - capacitance caused by the redox reaction of heteroatoms from nitrogen and oxygen in KACGS from the element analysis results, shown in Fig. S9. According to the pore size distribution of KACGS, the diameter of 0.8 nm is the optimum pore size for carbon-based electrodes for double-layer capacitance[30]. It is precisely that the pores with a diameter of 0.8 nm on the carbon nanosheets coated on both sides of graphene provide a suitable space for EDLC behavior and the hierarchical pore structure is beneficial for electrolyte penetration, thus resulting in such a high specific capacitance.

The triangular shapes of the curves have no change and the specific capacitance retains at a high level with the increasing of current density, suggesting a good rate capability. As shown in Fig. 5c, a very low R_s about 0.13 Ω can be observed from the expanded high-frequency region of the plots, suggesting that the KACGS electrode has good conductivity, which is attributed to the good intrinsic conductivity of graphene. The small diameter of the semicircle impedance loop in the high-frequency region could reflect the small charge transfer resistance (R_{ct} = 1.6 Ω)[31]. In the low-frequency region, the approximately vertical line shows the capacitive behavior of an ideal capacitor, due to the rapid ion diffusion in the electrolyte and EDLC behavior on the surface of electrode[32]. Stability is one of the most important properties of electrode materials for the supercapacitor. Cycling stability of KACGS was investigated at a current density of 5 A g^{-1} , shown in Fig. 5d. The assembled electrode of KACGS exhibits a quite good cycling stability. The specific capacitance can retain about 99.8% of the initial capacitance after 8 000 cycles. The stability of CGS was also supplied in Fig. S10, it also shows a stability but a low capacitance of 160 F g^{-1} at 1 A g^{-1}. The present KACGS electrode material exhibited better performance than many previously reported carbon materials (Table 1)[33–41]. The superior electrochemical performance of KACGS may be attributed to the hybrid advantages of advanced hierarchical pore structure and conductivity of graphene framework, boosting ion and electron transportation. (Fig. 6).

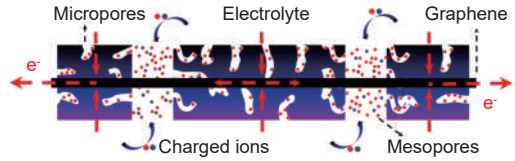

Fig. 6 Schematic showing rapid transport of electrons and charged ions effectively adsorbed in the layer of KACGS.

Table 1 Comparison of electrochemical performance of KACGS with some representative active carbon-based electrodes for supercapacitors (All were tested in three electrode system).

Electrode	Electrolyte	Specific capacitance (F g^{-1})	Ref.
Sandwich–like hierarchical porous carbon/graphene/carbon	6 mol L^{-1} KOH	324 (0.2 A g^{-1}) 224 (1A g^{-1})	This work
N-doped orderedmesoporous carbon	6 mol L^{-1} KOH	227 (0.2 A g^{-1})	[33]
KOH-activated carbon	6 mol L^{-1} KOH	152.6 (0.5 A g^{-1})	[34]
Hollow porous carbon spheres	6 mol L^{-1} KOH	303.9 (0.1 A g^{-1})	[35]
N-containing hierarchicalporous carbon spheres	7 mol L^{-1} KOH	276 (0.1 A g^{-1})	[36]
N/S-co-doped carbon nanobowls	6 mol L^{-1} KOH	279 (0.1 A g^{-1})	[37]
MXene-bonded activated carbon	1 mol L^{-1} Et_4NBF_4/AN	126 (0.1 A g^{-1})	[38]
N-doped mesoporous carbon	6 mol L^{-1} KOH	218 (0.5 A g^{-1})	[39]
3D Carbon aerogels	6 mol L^{-1} KOH	151 (0.5 A g^{-1})	[40]
Branched carbon nanotube/carbon nanofiber composite	1 mol L^{-1} H_2SO_4	207 (1 A g^{-1})	[41]

4 Conclusion

In summary, the sandwich-like hierarchical porous carbon/graphene/carbon architectures with controllable thickness were prepared by a directional polymerization approach. Abundant micropores in

RFC layers are beneficial to the rapid diffusion of electrolyte ions, which contribute to the double layer capacitance. Simultaneously, the graphene interlayers with good intrinsic conductivity could enhance the electrons transport during the charging and discharging processes. Such a unique integrated structure leads to excellent energy storage performance. The synthesized KACGS electrode delivers a high specific capacitance of 324 F g^{-1} at 0.2 A g^{-1}. Even at 5 A g^{-1}, the capacitance of 175 F g^{-1} can be still obtained after 8 000 cycles, showing a good cycling stability. It is believed that the hybrid structure can be applied to a wide range of applications requiring rapid electrons and ions transport.

Acknowledgements

National Natural Science Foundation of China (51902232, 52072275).

References

[1] Zhang L L, Zhao X S. Carbon-based materials as supercapacitor electrodes[J]. Chemical Society Reviews, 2009, 38(9): 2520-2531.

[2] Conway B E. Electrochemical Supercapacitors: Scientific Fundamentals and Technological Applications[M]. Springer Science & Business Media, 2013.

[3] Wang Y, Shi Z, Huang Y, et al. Supercapacitor devices based on graphene materials[J]. Journal of Physical Chemistry C, 2009, 113(30): 13103-13107.

[4] Zhang L L, Zhou R, Zhao X S. Graphene-based materials as supercapacitor electrodes[J]. Journal of Materials Chemistry, 2010, 20(29): 5983-5992.

[5] Chen H, Müller M B, Gilmore K J, et al. Mechanically strong, electrically conductive, and biocompatible graphene paper[J]. Advanced Materials, 2008, 20(18): 3557-3561.

[6] Kovalenko I, Bucknall D G, Yushin G. Detonation nanodiamond and onion-like-carbon-embedded polyaniline for supercapacitors[J]. Advanced Functional Materials, 2010, 20(22): 3979-3986.

[7] Xie Q, Zhou S, Zheng A, et al. Sandwich-like nitrogen-enriched porous carbon/graphene composites as electrodes for aqueous symmetric supercapacitors with high energy density[J]. Electrochimica Acta, 2016, 189: 22-31.

[8] Zhang J, Zhao X S. Conducting polymers directly coated on reduced graphene oxide sheets as high-performance supercapacitor electrodes[J]. The Journal of Physical Chemistry C, 2012, 116(9): 5420-5426.

[9] Liu A, Li C, Bai H, et al. Electrochemical deposition of polypyrrole/sulfonated graphene composite films[J]. Journal of Physical Chemistry C, 2010, 114(51): 22783-22789.

[10] Zhao Y, Zhang Z, Ren Y, et al. Vapor deposition polymerization of aniline on 3D hierarchical porous carbon with enhanced cycling stability as supercapacitor electrode[J]. Journal of Power Sources, 2015, 286: 1-9.

[11] Wang Y, Song Y, Xia Y. Electrochemical capacitors: Mechanism, materials, systems, characterization and applications[J]. Chemical Society Reviews, 2016, 45(21): 5925-5950.

[12] Huang Y, Tao J, Meng W, et al. Super-high rate stretchable polypyrrole-based supercapacitors with excellent cycling stability[J]. Nano Energy, 2015, 11: 518-525.

[13] Snook G A, Kao P, Best A S. Conducting-polymer-based supercapacitor devices and electrodes[J]. Journal of Power Sources, 2011, 196(1): 1-12.

[14] Wang L, Sun L, Tian C, et al. A novel soft template strategy to fabricate mesoporous carbon/graphene composites as high-performance supercapacitor electrodes[J]. RSC Advances, 2012, 2(22): 8359-8367.

[15] Pei F, Lin L, Ou D, et al. Self-supporting sulfur cathodes enabled by two-dimensional carbon yolk-shell nanosheets for high-energy-density lithium-sulfur batteries[J]. Nature Communications, 2017, 8(1): 482-491.

[16] Zhu J, Yang X, Fu Z, et al. Three-dimensional macroassembly of sandwich-like, hierarchical, porous carbon/graphene nanosheets towards ultralight, superhigh surface area, multifunctional aerogels[J]. Chemistry, 2016, 22(7): 2515-2524.

[17] Hao G P, Lu A H, Dong W, et al. Sandwich-type microporous carbon nanosheets for enhanced supercapacitor performance[J]. Advanced Energy Materials, 2013, 3(11): 1421-1427.

[18] Humers W, Offeman R. Preparation of graphitic oxide[J]. Journal of American Chemical Society, 1958, 80(6): 1334-1339.

[19] Lei Q, Song H, Zhou D, et al. Morphology control and supercapacitor performance of resorcinol –formaldehyde-based carbon particles upon Ni loading in an inverse emulsion system[J]. RSC Advances, 2015, 5(96): 78526-78533.

[20] Zheng C, Zhou X, Cao H, et al. Synthesis of porous graphene/activated carbon composite with high packing density and large specific surface area for supercapacitor electrode material[J]. Journal of Power Sources, 2014, 258: 290-296.

[21] Jäckel N, Rodner M, Schreiber A, et al. Anomalous or regular capacitance? The influence of pore size dispersity on double-layer formation[J]. Journal of Power Sources, 2016, 326: 660-671.

[22] Lu W, Liu M, Miao L, et al. Nitrogen-containing ultramicroporous carbon nanospheres for high performance supercapacitor electrodes[J]. Electrochimica Acta, 2016, 205: 132-141.

[23] Li D, Zhang L, Chen H, et al. Graphene-based nitrogen-doped carbon sandwich nanosheets: a new capacitive process controlled anode material for high-performance sodium-ion batteries[J]. Journal of Materials Chemistry A, 2016, 4(22): 8630-8635.

[24] Sadezky A, Muckenhuber H, Grothe H, et al. Raman microspectroscopy of soot and related carbonaceous materials: Spectral analysis and structural information[J]. Carbon, 2005, 43(8): 1731-1742.

[25] Yang D, Bock C. Laser reduced graphene for supercapacitor applications[J]. Journal of Power Sources, 2017, 337: 73-81.

[26] Yuan K, Hu T, Xu Y, et al. Nitrogen-doped porous carbon/graphene nanosheets derived from two-dimensional conjugated microporous polymer sandwiches with promising capacitive performance[J]. Materials Chemistry Frontiers, 2017, 1(2): 278-285.

[27] Wu S, Chen G, Kim N Y, et al. Creating pores on graphene platelets by low-temperature KOH activation for enhanced electrochemical performance[J]. Small, 2016, 12(17): 2376-2384.

[28] Inal I I G, Holmes S M, Banford A, et al. The performance of supercapacitor electrodes developed from chemically activated carbon produced from waste tea[J]. Applied Surface Science, 2015, 357: 696-703.

[29] Yang X, Fu Z, Jiao X, et al. Preparation and study of ultra-low density carbon aerogel[J]. Atomic Energy Science and Technology, 2012, 46(8): 996-1000.

[30] Galhena D T, Bayer B C, Hofmann S, et al. Understanding capacitance variation in sub-nanometer pores by in situ tuning of interlayer constrictions[J]. ACS nano, 2015, 10(1): 747-754.

[31] Li W, Zhang F, Dou Y, et al. A self-template strategy for the synthesis of mesoporous carbon nanofibers as advanced supercapacitor electrodes[J]. Advanced Energy Materials, 2011, 1(3): 382-386.

[32] Huang Z D, Zhang B, Liang R, et al. Effects of reduction process and carbon nanotube content on the supercapacitive performance of flexible graphene oxide papers[J]. Carbon, 2012, 50(11): 4239-4251.

[33] Wei J, Zhou D, Sun Z, et al. A controllable synthesis of rich nitrogen-doped ordered mesoporous carbon for CO2 capture and supercapacitors[J]. Advanced Functional Materials, 2013, 23(18): 2322-2328.

[34] Yu M, Li J, Wang L. KOH-activated carbon aerogels derived from sodium carboxymethyl cellulose for high-performance supercapacitors and dye adsorption[J]. Chemical Engineering Journal, 2017, 310: 300-306.

[35] Liu J, Wang X, Gao J, et al. Hollow porous carbon spheres with hierarchical nanoarchitecture for application of the high performance supercapacitors[J]. Electrochimica Acta, 2016, 211: 183-192.

[36] Pang J, Zhang W, Zhang H, et al. Sustainable nitrogen-containing hierarchical porous carbon spheres derived from sodium lignosulfonate for high-performance supercapacitors[J]. Carbon, 2018, 132: 280-293.

[37] Wang J G, Liu H, Zhang X, et al. Elaborate construction of N/S-co-doped carbon nanobowls for ultrahigh-power supercapacitors[J]. Journal of Materials Chemistry A, 2018, 6(36): 17653-17661.

[38] Yu L, Hu L, Anasori B, et al. MXene-bonded activated carbon as a flexible electrode for high-performance supercapacitors[J]. ACS Energy Letters, 2018, 3(7): 1597-1603.

[39] Wu K, Liu Q. Nitrogen-doped mesoporous carbons for high performance supercapacitors[J]. Applied Surface Science, 2016, 379: 132-139.

[40] Xu Y, Ren B, Wang S, et al. Carbon aerogel-based supercapacitors modified by hummers oxidation method[J]. Journal of Colloid and Interface Science, 2018, 527: 25-32.

[41] Zhou Y, Zhou X, Ge C, et al. Branched carbon nanotube/carbon nanofiber composite for supercapacitor electrodes[J]. Materials Letters, 2019, 246: 174-177.